ONE-DIMENSIONAL FINITE DIFFERENCE SCHEMES TO IMPLEMENT THE SPLITTING METHOD FOR AXISYMMETRIC EQUATIONS IN THE DYNAMICS OF ELASTIC MEDIUM

V. M. Sadovskii[1], O. V. Sadovskaya[2], and E. A. Efimov[3]

We construct efficient finite difference shock-capturing schemes for the solution of direct seismic problems in axisymmetric formulation. When parallelizing the algorithms implementing the schemes on multiprocessor computing systems, the two-cyclic splitting method with respect to the spatial variables is used. One-dimensional systems of equations are solved at the stages of splitting on the basis of explicit grid-characteristic schemes and an implicit finite difference scheme of the "predictor–corrector" type with controlled artificial energy dissipation. The verification of algorithms and programs is fulfilled on the exact solutions of one-dimensional problems describing traveling monochromatic waves. The comparison of the results showed the advantages of the scheme with controlled energy dissipation in terms of the accuracy of computing smooth solutions and the advisability of application of explicit monotone schemes when calculating discontinuities.

---

1. Introduction. When performing numerical modeling of seismic wave propagation in plane layered soil masses under the action of localized pulse or periodic perturbations, it is advisable to apply methods taking into account axial symmetry of the problems. Compared to three-dimensional spatial formulation of the problem, this enables a reduction of computational costs, with a negligible loss in precision caused by heterogeneity of coefficients in the constitutive equations (dependence of coefficients on the radius). In the case of several sources of disturbances acting together, either synchronously or with some time lag, the desired wave fields can be constructed by superimposing axisymmetric fields generated by individual sources. We apply this approach in our works on mathematical modeling of electromagnetic seismic pulse source Yenisei [1–3].

The key problem in the development of computational algorithms for solving axisymmetric problems is the proper selection of ways to approximate lowest terms in the equations of dynamic theory of elasticity written in the cylindrical coordinate system, which cause decay of the equations along the axis of symmetry. Our goal is to choose the right method, while remaining within the framework of the technology for constructing the Godunov conservative discontinuity decomposition scheme [4, 5], which has proven itself in solving plane and spatial problems of dynamic theory of elasticity, in modeling different resistance to compression and tension of granular and porous materials [6–9], wave propagation and cracking in blocky media [10–13] and other nonlinear processes.

Previously, methods for solving axisymmetric equations of dynamics of elastic media were developed and applied by many authors. In [14], a method of characteristics was implemented to analyze one-dimensional motions with cylindrical waves. Grid-characteristic methods for solving spatial problems were developed in [15–17]. Finite difference schemes for solving the plane problem equations and spatial equations based on the characteristic method, which allow calculating the discontinuities of velocities and stresses, were proposed in [18–20]. In [21–23] these methods were applied to the analysis of wave processes in linearly elastic, viscoelastic and elastic-plastic media. Methods based on axisymmetric equations were used in the numerical simulation of the dynamics of rotational plates and shells in [24–28].

---

[1] Institute of Computational Modeling, Siberian Branch of Russian Academy of Sciences; Akademgorodok 50/44, Krasnoyarsk, 660036, Russia; Dr. Sci., Professor, Director, e-mail: sadov@icm.krasn.ru

[2] Institute of Computational Modeling, Siberian Branch of Russian Academy of Sciences; Akademgorodok 50/44, Krasnoyarsk, 660036, Russia; Ph.D., Senior Scientist, e-mail: o_sadov@icm.krasn.ru

[3] Siberian Federal University, School of Mathematics and Computer Science; Svobodny prospekt 79, Krasnoyarsk, 660041, Russia; Postgraduate, e-mail: eugene6467@mail.ru

2. Equations of axisymmetric motion. The equations of dynamic elasticity theory with axial symmetry in velocities and stresses can be written in the form of the following system:

$$\rho\, r\, \frac{\partial v_r}{\partial t} = \frac{\partial(r\,\sigma_r)}{\partial r} + \frac{\partial(r\,\sigma_{rz})}{\partial z} - \sigma_\varphi\,, \quad \rho\, r\, \frac{\partial v_\varphi}{\partial t} = \frac{\partial(r\,\sigma_{r\varphi})}{\partial r} + \frac{\partial(r\,\sigma_{\varphi z})}{\partial z} + \sigma_{r\varphi}\,,$$

$$\rho\, r\, \frac{\partial v_z}{\partial t} = \frac{\partial(r\,\sigma_{rz})}{\partial r} + \frac{\partial(r\,\sigma_z)}{\partial z}\,, \qquad \frac{1}{E}\frac{\partial \sigma_r}{\partial t} - \frac{\nu}{E}\frac{\partial}{\partial t}\big(\sigma_\varphi + \sigma_z\big) = \frac{\partial v_r}{\partial r}\,,$$

$$\frac{1}{E}\frac{\partial \sigma_\varphi}{\partial t} - \frac{\nu}{E}\frac{\partial}{\partial t}\big(\sigma_z + \sigma_r\big) = \frac{v_r}{r}\,, \qquad \frac{1}{E}\frac{\partial \sigma_z}{\partial t} - \frac{\nu}{E}\frac{\partial}{\partial t}\big(\sigma_r + \sigma_\varphi\big) = \frac{\partial v_z}{\partial z}\,, \qquad (1)$$

$$\frac{1}{\mu}\frac{\partial \sigma_{r\varphi}}{\partial t} = \frac{\partial v_\varphi}{\partial r} - \frac{v_\varphi}{r}\,, \qquad\qquad \frac{1}{\mu}\frac{\partial \sigma_{rz}}{\partial t} = \frac{\partial v_z}{\partial r} + \frac{\partial v_r}{\partial z}\,, \qquad\qquad \frac{1}{\mu}\frac{\partial \sigma_{\varphi z}}{\partial t} = \frac{\partial v_\varphi}{\partial z}\,.$$

Here ρ is the density of the medium, $E = 2\,\mu\,(1 + \nu)$ is Young's modulus, μ and ν are the shear modulus and Poisson's ratio; the r and z axes of the cylindrical coordinate system are directed along the radius and the axis of symmetry, respectively. This form of notation is convenient for deriving the energy balance equation. In order to accomplish this, it is necessary to multiply the equations of motion by v_r, v_φ, v_z and to multiply the constitutive equations by $r\sigma_r$, $r\sigma_\varphi$, $r\sigma_z$, $r\sigma_{r\varphi}$, $r\sigma_{rz}$, $r\sigma_{\varphi z}$, respectively, and then to sum the right and left-hand sides of the equations. We arrive at the following equality:

$$\frac{\partial}{\partial t}\left(\rho\, r\, \frac{v_r^2 + v_\varphi^2 + v_z^2}{2} + r\, W\right) = \frac{\partial}{\partial r}\Big(r\, v_r\, \sigma_r + r\, v_\varphi\, \sigma_{r\varphi} + r\, v_z\, \sigma_{rz}\Big) + \frac{\partial}{\partial z}\Big(r\, v_r\, \sigma_{rz} + r\, v_\varphi\, \sigma_{\varphi z} + r\, v_z\, \sigma_z\Big)\,, \quad (2)$$

where W is the elastic potential that can be represented as the quadratic form with respect to the stresses:

$$4\,\mu\, W = \sigma_r^2 + \sigma_\varphi^2 + \sigma_z^2 + 2\,\sigma_{r\varphi}^2 + 2\,\sigma_{rz}^2 + 2\,\sigma_{\varphi z}^2 - \frac{\nu}{1+\nu}\big(\sigma_r + \sigma_\varphi + \sigma_z\big)^2\,.$$

The system expressed by (1) is hyperbolic. It can be decomposed into the following two independent subsystems: the first subsystem consists of the equations whose numbers counted from left to right are 1, 3, 4, 5, 6, and 8 and describes the planar motion, whereas the second one (equations 2, 7, and 9) describes the torsional motion. The planar motion is a superposition of longitudinal and transverse waves propagating with the velocities

$$c_p = \sqrt{\frac{2\,\mu}{\rho}\, \frac{1 - \nu}{1 - 2\,\nu}}\,, \quad c_s = \sqrt{\frac{\mu}{\rho}}\,,$$

respectively. The torsional waves propagate with the velocity c_s.

When studying seismic problems, we apply the method of two-cyclic splitting by spatial variables to the solution of (1), in which a series of one-dimensional problems are solved at different stages in parallel mode. The advantage of two-cyclic splitting method compared to the usual splitting method (the total approximation method) is that it preserves the second order of accuracy when using second-order difference schemes to solve one-dimensional systems [29]. Numerical implementation of the stages of the splitting method in the direction of the symmetry axis z does not cause any difficulties, since after reducing the corresponding one-dimensional equations by r we arrive at a system of equations with constant coefficients; this system can be decomposed into subsystems describing the plane longitudinal and transverse elastic waves. The Godunov discontinuity decomposition scheme [4] or the grid-characteristic difference scheme with limiting reconstruction of Riemann invariants [30] (based on the same idea) are both applicable to their solution.

The one-dimensional system of equations in the direction of the radial axis r is decomposed into three subsystems describing the longitudinal, transverse, and torsional waves. The direct application of standard finite difference schemes based on the approximation of equations in the plane elasticity problem with addition of derivative-free terms leads to undesirable effects such as asymptotic instability with accumulation of rounding errors during calculations with a large number of time steps or to momentum and energy disbalances. This calls into question the reliability of the numerical results obtained.

A universal way to deal with such effects is to use the fully conservative finite difference schemes [31, 32] in combination with the artificial viscosity method [33]; this method allows one to smooth the oscillations of numerical solutions when calculating discontinuities due to the schematic energy dissipation. For the dynamic elasticity theory equations, a general approach to constructing conservative numerical methods with controlled energy dissipation was developed by Ivanov [34, 35]. This approach can be applied to subsystems of equations describing the one-dimensional motions of an elastic medium with longitudinal, transverse, and torsional cylindrical waves.

3. Longitudinal cylindrical waves. The longitudinal wave equations can be written in an equivalent form via the Lamé elasticity parameters $\lambda = 2\mu\nu/(1-2\nu)$ and μ:

$$\rho\, r\, \frac{\partial v_r}{\partial t} = \frac{\partial(r\,\sigma_r)}{\partial r} - \sigma_\varphi\,, \qquad \frac{\partial \sigma_r}{\partial t} = (\lambda + 2\,\mu)\,\frac{\partial v_r}{\partial r} + \lambda\,\frac{v_r}{r}\,,$$

$$\frac{\partial \sigma_\varphi}{\partial t} = \lambda\,\frac{\partial v_r}{\partial r} + (\lambda + 2\,\mu)\,\frac{v_r}{r}\,, \quad \frac{\partial \sigma_z}{\partial t} = \lambda\left(\frac{\partial v_r}{\partial r} + \frac{v_r}{r}\right). \tag{3}$$

The energy balance equation (2) for this system takes the following form:

$$\frac{\partial}{\partial t}\left(\rho\, r\,\frac{v_r^2}{2} + r\,W\right) = \frac{\partial(r\,v_r\,\sigma_r)}{\partial r}\,.$$

The integration of (3) over a spatial-temporal rectangular grid leads to the following discrete equations of the "corrector" step:

$$\rho\, r^0\,\frac{\hat{v}_r - v_r}{\tau} = \frac{r^+\sigma_r^+ - r^-\sigma_r^-}{h} - \sigma_\varphi^0\,, \qquad \frac{\hat{\sigma}_r - \sigma_r}{\tau} = (\lambda + 2\,\mu)\,\frac{v_r^+ - v_r^-}{h} + \lambda\,\frac{v_r^0}{r^0}\,,$$

$$\frac{\hat{\sigma}_\varphi - \sigma_\varphi}{\tau} = \lambda\,\frac{v_r^+ - v_r^-}{h} + (\lambda + 2\,\mu)\,\frac{v_r^0}{r^0}\,, \quad \frac{\hat{\sigma}_z - \sigma_z}{\tau} = \lambda\,\frac{v_r^+ - v_r^-}{h} + \lambda\,\frac{v_r^0}{r^0}\,, \tag{4}$$

where the capped values refer to the middle of cells in the upper time layer, whereas the uncapped values refer to the middle of cells in the lower layer; the values with "$\pm$" upper indices refer to the right and left cell boundaries; $r^0 = (r^+ + r^-)/2$. The velocity v_r^0 and the stress σ_φ^0 as well as the values $\sigma_r^\pm$ and $v_r^\pm$ are defined at the "predictor" step.

The difference analogue of the energy balance equation (2) for longitudinal waves is obtained by multiplying equations (4) by $(\hat{v}_r + v_r)/2$ and $r^0(\hat{\sigma}_r + \sigma_r)/2$, $r^0(\hat{\sigma}_\varphi + \sigma_\varphi)/2$, $r^0(\hat{\sigma}_z + \sigma_z)/2$, respectively:

$$\rho\, r^0\,\frac{\hat{v}_r^2 - v_r^2}{2\,\tau} + r^0\,\frac{\hat{W} - W}{\tau} = \frac{r^+ v_r^+ \sigma_r^+ - r^- v_r^- \sigma_r^-}{h} - D\,,$$

$$D = \frac{r^+\sigma_r^+ - r^-\sigma_r^-}{h}\left(\frac{v_r^+ + v_r^-}{2} - \frac{\hat{v}_r + v_r}{2}\right)$$

$$+ \frac{v_r^+ - v_r^-}{h}\left(\frac{r^+\sigma_r^+ + r^-\sigma_r^-}{2} - r^0\,\frac{\hat{\sigma}_r + \sigma_r}{2}\right) + \sigma_\varphi^0\,\frac{\hat{v}_r + v_r}{2} - v_r^0\,\frac{\hat{\sigma}_\varphi + \sigma_\varphi}{2}\,.$$

The idea of controlled energy dissipation [34] is that the expression for D is given explicitly as a positive-definite quadratic form. This form can be identically equal to zero. Then, a nondissipative (fully conservative) scheme is obtained.

Now we take the quadratic form as $D = \gamma\,(v_r^+ - v_r^-)^2/h^2$ with a free parameter $\gamma \geqslant 0$ and assume that

$$v_r^0 = \frac{\hat{v}_r + v_r}{2} = \frac{\hat{v}_r^+ + v_r^-}{2}\,, \quad \sigma_\varphi^0 = \frac{\hat{\sigma}_\varphi + \sigma_\varphi}{2} = \frac{\sigma_\varphi^+ + \sigma_\varphi^-}{2}\,, \quad \frac{r^+\sigma_r^+ + r^-\sigma_r^-}{2} - r^0\,\frac{\hat{\sigma}_r + \sigma_r}{2} = \gamma\,\frac{v_r^+ - v_r^-}{h}\,. \tag{5}$$

In this case, the artificial energy dissipation is non-negative, which automatically ensures the stability of computations; this dissipation decreases with grid refinement and depends only on the medium strain rate. If $\gamma = 0$, then the scheme is fully conservative and the energy conservation law is fulfilled at the discrete level in this scheme. In practice, however, it is not suitable for calculating discontinuous solutions and solutions with large gradients because of its non-monotonicity.

Taking into account (4), we can reduce the closing equations of the scheme with controlled energy dissipation used to calculate the values with "$\pm$" indices at the "predictor" step to the following system:

$$r^+\sigma_r^+ - r^-\sigma_r^- = a_{j-1/2}\,v_r^+ + b_{j-1/2}\,v_r^- + f_{j-1/2}\,, \quad r^+\sigma_r^+ + r^-\sigma_r^- = c_{j-1/2}\,v_r^+ + d_{j-1/2}\,v_r^- + g_{j-1/2}\,.$$

Here $a_{j-1/2}$, $b_{j-1/2}$, $c_{j-1/2}$, $d_{j-1/2}$, $f_{j-1/2}$, and $g_{j-1/2}$ are the coefficients dependent on the cell number $j = 1, 2, \ldots, n$ (the fractional indices refer to the centers of cells):

$$a_{j-1/2} = \frac{\rho\, h\, r^0}{\tau} + (\lambda + 2\,\mu)\,\frac{\tau\, h}{4\, r^0} + \lambda\,\frac{\tau}{2}\,, \quad b_{j-1/2} = \frac{\rho\, h\, r^0}{\tau} + (\lambda + 2\,\mu)\,\frac{\tau\, h}{4\, r^0} - \lambda\,\frac{\tau}{2}\,, \quad f_{j-1/2} = h\,\sigma_\varphi - 2\,h\, r^0\,\frac{\rho\, v_r}{\tau}\,,$$

$$c_{j-1/2} = \lambda\,\frac{\tau}{2} + (\lambda + 2\,\mu)\,\frac{\tau\, r^0}{h} + \frac{2\,\gamma}{h}\,, \qquad d_{j-1/2} = \lambda\,\frac{\tau}{2} - (\lambda + 2\,\mu)\,\frac{\tau\, r^0}{h} - \frac{2\,\gamma}{h}\,, \qquad g_{j-1/2} = 2\, r^0 \sigma_r\,.$$

Hence,

$$2\,r^+\sigma_r^+ = \left(a_{j-1/2} + c_{j-1/2}\right) v_r^+ + \left(b_{j-1/2} + d_{j-1/2}\right) v_r^- + f_{j-1/2} + g_{j-1/2}\,,$$
$$2\,r^-\sigma_r^- = \left(c_{j-1/2} - a_{j-1/2}\right) v_r^+ + \left(d_{j-1/2} - b_{j-1/2}\right) v_r^- + g_{j-1/2} - f_{j-1/2}\,. \tag{6}$$

Equating these expressions after shifting by the index j, we arrive at the following tridiagonal system of equations to determine the velocities $v_r^+ = v_r^j$ and $v_r^- = v_r^{j-1}$ at the cell boundaries:

$$A_j\, v_r^{j+1} + C_j\, v_r^j + B_j\, v_r^{j-1} = F_j\,, \tag{7}$$

where

$$A_j = c_{j+1/2} - a_{j+1/2}\,, \qquad C_j = d_{j+1/2} - b_{j+1/2} - a_{j-1/2} - c_{j-1/2}\,,$$
$$B_j = -\,b_{j-1/2} - d_{j-1/2}\,, \quad F_j = f_{j+1/2} + f_{j-1/2} - g_{j+1/2} + g_{j-1/2}\,.$$

The boundary condition $v_r^0 = 0$ is added to the system of equations for internal nodes (7) on the symmetry axis and the boundary condition $v_r^n = v$ is also added if the velocity v of particles is given on the right boundary $r = R$ or the condition

$$\left(a_{n-1/2} + c_{n-1/2}\right) v_r^n + \left(b_{n-1/2} + d_{n-1/2}\right) v_r^{n-1} + f_{n-1/2} + g_{n-1/2} = 2\,R\sigma,$$

resulting from (6) is also added if the external stress σ is given at the boundary. In both these cases, the system of equations with boundary conditions is solved by the Thomas algorithm.

Thus, the algorithm of transition to a new temporal layer in the numerical implementation of the scheme begins with the calculation of the values $v_r^{\pm}$ and $\sigma_r^{\pm}$ using equations (6) and (7) of the "predictor" step and, then, v_r^0 and σ_φ^0 can be determined by (5). The final calculations of $\hat{v}_r$, $\hat{\sigma}_r$, $\hat{\sigma}_\varphi$ and $\hat{\sigma}_z$ are based on equations (4) of the "corrector" step.

For comparison, let us consider three variants of explicit finite difference schemes based on the solution of the problem on disappearance of an arbitrary discontinuity. The schemes are constructed by approximating the first equation in system (3) written in an equivalent (non-conservative) form:

$$\rho\,\frac{\partial v_r}{\partial t} = \frac{\partial \sigma_r}{\partial r} + \frac{\sigma_r - \sigma_\varphi}{r}\,.$$

The "predictor–corrector" scheme with explicit approximation of the lowest terms

$$\rho\,\frac{\hat{v}_r - v_r}{\tau} = \frac{\sigma_r^+ - \sigma_r^-}{h} + \frac{\sigma_r - \sigma_\varphi}{r^0}\,, \qquad \frac{\hat{\sigma}_r - \sigma_r}{\tau} = (\lambda + 2\,\mu)\,\frac{v_r^+ - v_r^-}{h} + \lambda\,\frac{v_r}{r^0}\,,$$

$$\frac{\hat{\sigma}_\varphi - \sigma_\varphi}{\tau} = \lambda\,\frac{v_r^+ - v_r^-}{h} + (\lambda + 2\,\mu)\,\frac{v_r}{r^0}\,, \quad \frac{\hat{\sigma}_z - \sigma_z}{\tau} = \lambda\left(\frac{v_r^+ - v_r^-}{h} + \frac{v_r}{r^0}\right),$$

$$v_r^+ - \frac{\sigma_r^+}{\rho\,c_p} = v_r - \frac{\sigma_r}{\rho\,c_p}\,, \qquad\qquad v_r^- + \frac{\sigma_r^-}{\rho\,c_p} = v_z + \frac{\sigma_r}{\rho\,c_p}$$

is suitable for calculations only if the Courant number $K_p = c_p\,\tau/h$ belongs to the range from 0 to 0.8. When this number is greater than 0.8, parasitic oscillations appear near the axis of symmetry. The oscillations grow in amplitude indefinitely with increasing K_p from 0.9 to 1, which results in a distortion of the solution. If K_p is small, then the numerical viscosity leads to the situation when the solution becomes oversmoothed. For these two reasons, this scheme is not advisable to use in these calculations.

The scheme with implicit approximation of the lowest terms is obtained by substituting the stresses σ_r, σ_φ and the velocity v_r in the lowest terms with $\hat{\sigma}_r$, $\hat{\sigma}_\varphi$ and $\hat{v}_r$. This scheme is stable and monotonic over the whole range $0 < K_p \leqslant 1$, but it also has an excessive smoothing effect due to the scheme viscosity when the Courant number is sufficiently small.

The implicit Crank–Nicolson approximation scheme with the replacement of σ_r, σ_φ and v_r by

$$\frac{\hat{\sigma}_r + \sigma_r}{2}\,, \quad \frac{\hat{\sigma}_\varphi + \sigma_\varphi}{2}\,, \quad \frac{\hat{v}_r + v_r}{2}$$

has advantages over the explicit and implicit schemes with respect to the accuracy of numerical solution.

The computational algorithms implementing the schemes were verified by comparing the numerical results with the exact solution describing monochromatic waves of a prescribed frequency ω. This exact solution can be obtained by separation of variables:

$$v_r = \frac{\sigma_0}{\rho\, c_p} \sin\omega t\, J_1(\xi_p)\,, \qquad \sigma_r = \frac{\sigma_0}{\lambda + 2\,\mu}\cos\omega t\left((\lambda + 2\,\mu)\, J_2(\xi_p) - \frac{2\,(\lambda + \mu)}{\xi_p}\, J_1(\xi_p)\right),$$

$$\sigma_\varphi = \frac{\sigma_0}{\lambda + 2\,\mu}\cos\omega t\left(\lambda\, J_2(\xi_p) - \frac{2\,(\lambda + \mu)}{\xi_p}\, J_1(\xi_p)\right), \qquad \sigma_z = \frac{\lambda\, \sigma_0}{\lambda + 2\,\mu}\cos\omega t\left(J_2(\xi_p) - \frac{2}{\xi}\, J_1(\xi_p)\right),$$

where $\xi_p = \omega\, r/c_p$ is a dimensionless variable and $J_k(x)$ are the Bessel functions of integer order k.

Tables 1–4 show the relative errors of the schemes for different frequencies depending on the Courant number. In these calculations, the dimensionless frequency $\bar{\omega} = \omega\, R/c_s$ (where R is the radius of the computational domain) varied from 10 to 50. At these frequencies, the number of half-waves in the computational domain varies from one and a half to seven and a half (Fig. 1).

The errors of numerical solution were calculated relative to the discrete analog of the norm of the space $L_\infty\big(0, T; L_2(0, R)\big)$:

$$\big\|(v_r, \sigma_r, \sigma_\varphi, \sigma_z)\big\| = \sup_{0 < t < T}\sqrt{\pi\int_0^R\left(\rho\,\frac{v_r^2}{2} + W\right)dr^2}\,.$$

Table 1

Relative errors for the nondissipative scheme: $\gamma = 0$ (longitudinal waves)

K_p \ $\bar{\omega}$	10	20	30	40	50
0.5	0.00023	0.00110	0.00837	0.01408	0.03500
0.75	0.00009	0.00045	0.00405	0.00701	0.01818
1	0.00019	0.00081	0.00201	0.00349	0.00563
1.25	0.00049	0.00210	0.00977	0.01621	0.03527
1.5	0.00085	0.00372	0.01920	0.03209	0.07125

Table 2

Relative errors for the scheme with explicit approximation of the lowest terms (longitudinal waves)

K_p \ $\bar{\omega}$	10	20	30	40	50
0.5	0.04334	0.09600	0.37513	0.40646	0.63148
0.75	0.02148	0.05053	0.19970	0.25226	0.39363

Table 3

Relative errors for the scheme with implicit approximation of the lowest terms (longitudinal waves)

K_p \ $\bar{\omega}$	10	20	30	40	50
0.5	0.04802	0.10547	0.39297	0.41076	0.65137
0.75	0.02860	0.06545	0.23341	0.26373	0.44424
1	0.01025	0.02666	0.03320	0.04613	0.05591

Table 4

Relative errors for the scheme with Crank–Nicolson approximation (longitudinal waves)

K_p \ $\bar{\omega}$	10	20	30	40	50
0.5	0.03824	0.09015	0.36576	0.40030	0.62509
0.75	0.01350	0.04288	0.18149	0.23903	0.37536
0.97	0.00912	0.02940	0.02788	0.05726	0.04975
1	0.01220	0.03379	0.05646	0.06663	0.12026
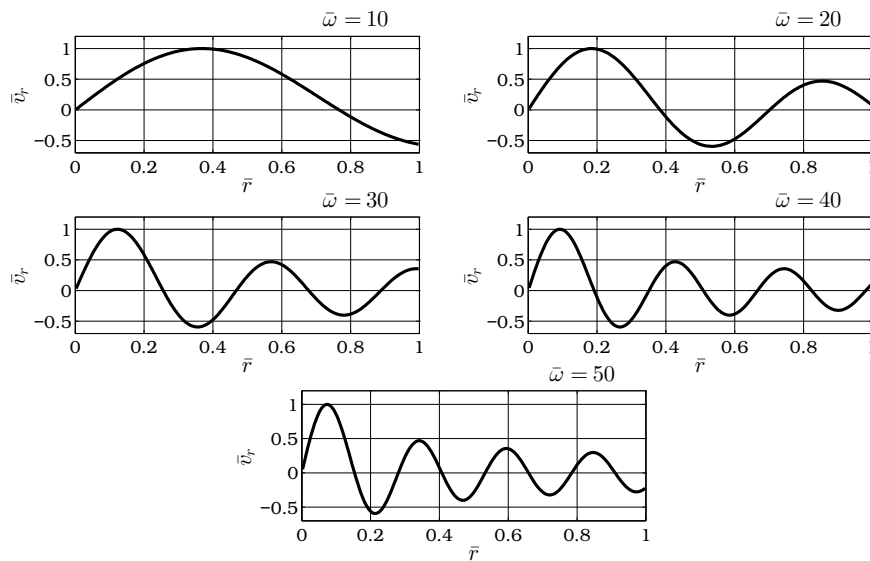
Figure 1. Exact solution with longitudinal cylindrical waves for dimensionless velocity

The time T was prescribed in such a way that, in the interval $(0, T)$, the longitudinal cylindrical wave passes the distance of $2R$ with a single reflection from the symmetry axis.

The calculations were performed on a finite difference grid of 200 cells. Our analysis of the table data shows that the numerical solution using the scheme with implicit approximation of the lowest terms and the scheme with Crank–Nicolson approximation loses accuracy if one half-wave contains less than 60–70 grid cells. The nondissipative scheme works well at all frequencies in the range being considered.

Figures 2 and 3 show the velocity profiles behind the front of a strong discontinuity caused by sudden
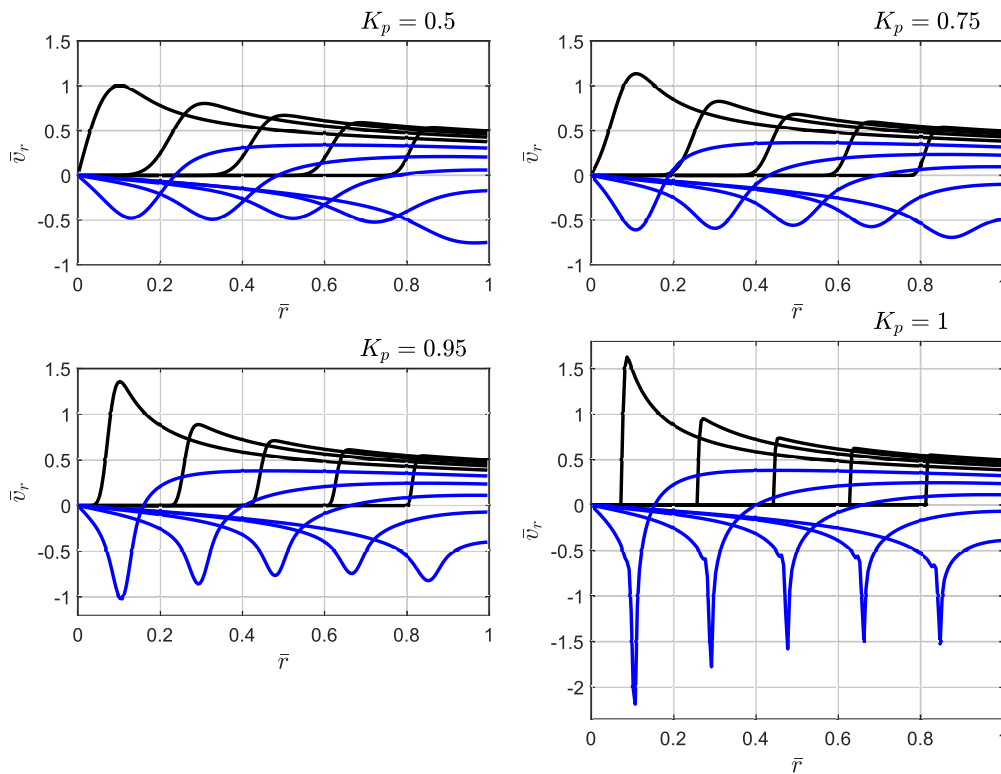
Figure 2. Velocity profiles behind the discontinuity front:
Crank–Nicolson approximation scheme (longitudinal waves)
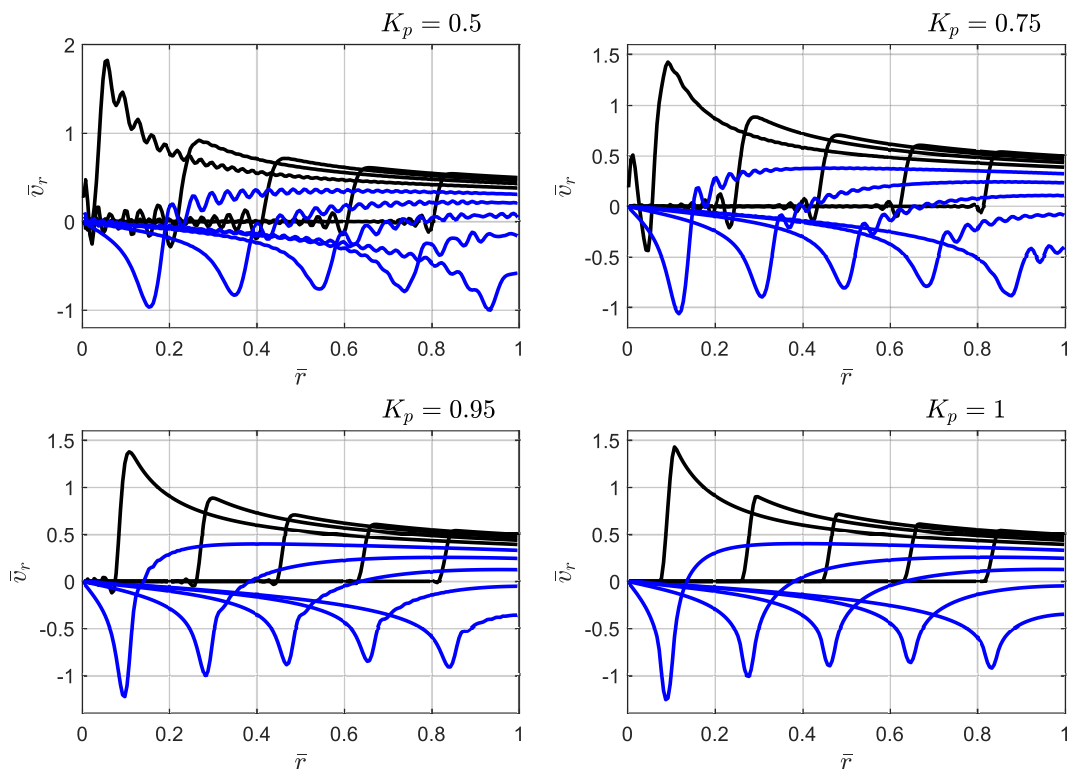
Figure 3. Velocity profiles behind the discontinuity front:
nondissipative scheme (longitudinal waves)

application of a constant stress at the domain boundary. The results shown in Fig. 2 are obtained by the Crank–Nicolson approximation scheme, in Fig. 3 — by the nondissipative scheme. In the case of the nondissipative scheme, the velocity and stress profiles are monotonic only for $K_p = 1$, but parasitic oscillations appear before the wave front for $K_p = 0.9$. These parasitic oscillations increase strongly as the Courant number deviates from the value of one. The oscillations can be smoothed by introducing the artificial energy dissipation and by selecting a certain value of the parameter $\gamma > 0$ or by smoothing the diagram of sharp stress application on the boundary by raising the stress level in a monotonic manner from zero to a specified constant value over at least 10 grid steps in time.

The smoothed velocity profiles obtained in the sudden loading calculations according to the controlled artificial energy dissipation scheme for $\gamma = 0.0005$ are shown in Fig. 4. We should note that the maximum wave amplitudes for fixed time moments on the plots are almost independent of the Courant number. This is an indicator of the scheme's good quality. When the Courant number changes, however, the position of the discontinuity front shifts slightly.

In order to parallelize computations on cluster architectures when solving the problems of large dimension on the basis of the controlled energy dissipation scheme, it is possible to apply an iterative process which has shown an exceptionally high rate of convergence in numerical experiments. As it turned out, it takes only two or three iterations to achieve the accuracy shown in Table 1.

The problem is to parallelize the Thomas algorithm at the "predictor" step of the finite difference scheme. In order to accomplish this, the system expressed by (7) should be first "broken" at the junctions of the neighboring processors and, then, the corresponding three-point equations of the system are replaced by the equations of Godunov's scheme with disappearance of discontinuities:

$$ v_r^j = \frac{v_{r\,j+1/2} + v_{r\,j-1/2}}{2} + \frac{\sigma_{r\,j+1/2} - \sigma_{r\,j-1/2}}{2\,\rho\,c_p}, $$

where the fractional indices indicate that the velocity and stress values belong to the boundary grid cells of neighboring processors. This procedure allows us to implement the Thomas algorithm on the processors of the computational cluster in the parallel mode and, thus, to obtain the first approximation of the solution. After
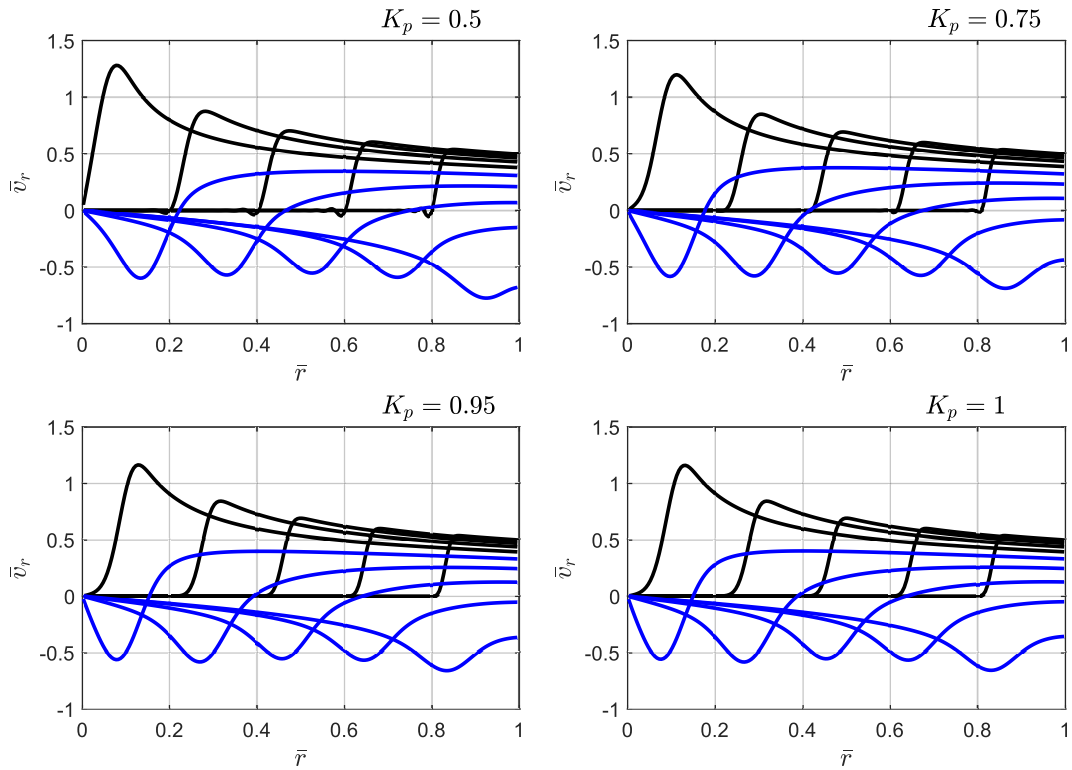
Figure 4. Velocity profiles behind the discontinuity front: scheme with dissipation (longitudinal waves)

that, we iteratively recalculate the velocity values at the processor junctions by the obtained approximation using the following formula:

$$\hat{v}_r^j = \frac{F_j - A_j\, v_r^{j-1} - B_j\, v_r^{j+1}}{C_j}$$

followed by a parallel implementation of the Thomas algorithm. With such an algorithm, the achieved calculation accuracy is almost completely restored for longitudinal wave equations after a single application of the algorithm described above. In the transverse wave and torsional wave problems considered below, another iteration is required to recover the calculation accuracy.

From the above figures it follows that the non-conservative difference scheme with the approximation of the lowest terms by the Crank–Nicolson method gives much more reliable results for the calculation of the discontinuous solutions in the whole range of variation of the Courant number $K_p \leqslant 1$, where this scheme is stable.

Note that similar schemes based on the equations in the conservative form (3) inadequately distort the picture of wave reflection from the symmetry axis even in the case of smooth solutions, which eventually results in the complete loss of accuracy.

The results of the studies discussed in this section are published in a short form in the authors' English-language paper [36].

4. Transverse cylindrical waves. In the axially symmetric case, the one-dimensional motions with transverse waves are described by the equations

$$\rho\, r\, \frac{\partial v_z}{\partial t} = \frac{\partial(r\, \sigma_{rz})}{\partial r}, \quad \frac{1}{\mu}\, \frac{\partial \sigma_{rz}}{\partial t} = \frac{\partial v_z}{\partial r}. \tag{8}$$

The following energy balance equation follows from (8):

$$\frac{\partial}{\partial t}\left(\rho\, r\, \frac{v_z^2}{2} + r\, \frac{\sigma_{rz}^2}{2\,\mu}\right) = \frac{\partial(r\, v_z\, \sigma_{rz})}{\partial r}.$$

When constructing a finite difference scheme with controlled energy dissipation, equations (8) are approximated by the following equations of the "corrector" step:

$$\rho\, r^0\, \frac{\hat{v}_z - v_z}{\tau} = \frac{r^+ \sigma_{rz}^+ - r^- \sigma_{rz}^-}{h}\,, \quad \frac{\hat{\sigma}_{rz} - \sigma_{rz}}{\mu\, \tau} = \frac{v_z^+ - v_z^-}{h}\,. \tag{9}$$

The discrete energy balance equation takes the following form:

$$\rho\, r^0\, \frac{\hat{v}_z^2 - v_z^2}{2\,\tau} + r^0\, \frac{\hat{\sigma}_{rz}^2 - \sigma_{rz}^2}{2\,\mu\,\tau} = \frac{r^+ v_z^+ \sigma_{rz}^+ - r^- v_z^- \sigma_{rz}^-}{h} - D\,,$$

$$D = \frac{r^+ \sigma_{rz}^+ - r^- \sigma_{rz}^-}{h}\left(\frac{v_z^+ + v_z^-}{2} - \frac{\hat{v}_z + v_z}{2}\right) + \frac{v_z^+ - v_z^-}{h}\left(\frac{r^+ \sigma_{rz}^+ + r^- \sigma_{rz}^-}{2} - r^0\, \frac{\hat{\sigma}_{rz} + \sigma_{rz}}{2}\right).$$

The scheme's artificial energy dissipation component is specified as the positive definite quadratic form $D = \gamma\,(v_z^+ - v_z^-)^2/h^2$ due to the closing equations of the "predictor" step:

$$\frac{\hat{v}_z + v_z}{2} = \frac{v_z^+ + v_z^-}{2}\,, \quad r^0\, \frac{\hat{\sigma}_{rz} + \sigma_{rz}}{2} = \frac{r^+ \sigma_{rz}^+ + r^- \sigma_{rz}^-}{2} - \gamma\, \frac{v_z^+ - v_z^-}{h} \tag{10}$$

(γ is a non-negative parameter of the scheme dissipation).

After eliminating the values $\hat{v}_z$ and $\hat{\sigma}_{rz}$ expressed from (9), equations (10) are transformed to the following system:

$$\frac{v_z^+ + v_z^-}{2} - \frac{\tau}{2\,\rho\, r^0}\, \frac{r^+ \sigma_{rz}^+ - r^- \sigma_{rz}^-}{h} = v_z\,, \quad \frac{r^+ \sigma_{rz}^+ + r^- \sigma_{rz}^-}{2} - \left(\gamma + \frac{\mu\,\tau\, r^0}{2}\right)\frac{v_z^+ - v_z^-}{h} = r^0\, \sigma_{rz}\,.$$

This system can be represented as

$$r^+ \sigma_{rz}^+ - r^- \sigma_{rz}^- = a_{j-1/2}\, v_z^+ + b_{j-1/2}\, v_z^- + f_{j-1/2}\,, \quad r^+ \sigma_{rz}^+ + r^- \sigma_{rz}^- = c_{j-1/2}\, v_z^+ + d_{j-1/2}\, v_z^- + g_{j-1/2}$$

with the following coefficients:

$$a_{j-1/2} = \frac{\rho\, h\, r^0}{\tau}\,, \qquad b_{j-1/2} = a_{j-1/2}\,, \qquad f_{j-1/2} = -2\, a_{j-1/2}\, v_z\,,$$

$$c_{j-1/2} = \mu\, \frac{\tau\, r^0}{h} + \frac{2\,\gamma}{h}\,, \quad d_{j-1/2} = -c_{j-1/2}\,, \quad g_{j-1/2} = 2\, r^0 \sigma_{rz}\,.$$

In these notations, the system of equations expressed by (6) is accurate up to the replacement of radial stress σ_r by the shear stress σ_{rz}. A boundary condition is added to this system on the symmetry axis:

$$(c_{1/2} - a_{1/2})v_z^1 + (d_{1/2} - b_{1/2})v_z^0 = f_{1/2} - g_{1/2}\,,$$

which corresponds to the condition $\sigma_{rz}^0 = 0$ for $r = 0$. The following boundary condition is also added at $r = R$ for the velocity $v_z^n = v$ or for the shear stress:

$$(a_{n-1/2} + c_{n-1/2})v_z^n + (b_{n-1/2} + d_{n-1/2})v_z^{n-1} = 2\, R\, \sigma - f_{n-1/2} - g_{n-1/2}\,.$$

With these boundary conditions, the resulting system of equations is solved by the Thomas algorithm; the corresponding algorithm for recalculating the solution per a single time step is the same as the algorithm used in the problem on longitudinal cylindrical waves.

In order to compare the accuracy of the numerical solution, we consider once again the three grid-characteristic schemes based on the equivalent representation of the system expressed by (8) in the form

$$\rho\, \frac{\partial v_z}{\partial t} = \frac{\partial \sigma_{rz}}{\partial r} + \frac{\sigma_{rz}}{r}\,, \quad \frac{1}{\mu}\, \frac{\partial \sigma_{rz}}{\partial t} = \frac{\partial v_z}{\partial r}$$

and on the approximation of these equations by the Godunov method with disappearance of discontinuities.

Numerical experiments show that the "predictor–corrector" scheme with the explicit approximation of the lowest terms

$$\rho\, \frac{\hat{v}_z - v_z}{\tau} = \frac{\sigma_{rz}^+ - \sigma_{rz}^-}{h} + \frac{\sigma_{rz}}{r^0}\,, \qquad \frac{\hat{\sigma}_{rz} - \sigma_{rz}}{\mu\, \tau} = \frac{v_z^+ - v_z^-}{h}\,,$$

$$v_z^+ - \frac{\sigma_{rz}^+}{\rho c_s} = v_z - \frac{\sigma_{rz}}{\rho c_s}\,, \qquad\qquad v_z^- + \frac{\sigma_{rz}^-}{\rho c_s} = v_z + \frac{\sigma_{rz}}{\rho c_s} \tag{11}$$

is stable if the Courant–Friedrichs–Lewy stability condition is fulfilled: $K_s \equiv c_s \tau / h \leqslant 1$; however, this sheme is not monotonic for the maximum allowed time step $\tau = h/c_s$ (parasitic oscillations appear near the symmetry axis). If the time step is small, then the numerical viscosity leads to the situation when the solution becomes oversmoothed.

The scheme with implicit approximation of the lowest terms can be obtained by replacing the first equation of (11) by the equation

$$\rho \frac{\hat{v}_z - v_z}{\tau} = \frac{\sigma_{rz}^+ - \sigma_{rz}^-}{h} + \frac{\hat{\sigma}_{rz}}{r^0} \ .$$

This scheme is stable over the entire range $0 < K_s \leqslant 1$ and also shows the smoothing property when calculating discontinuous solutions for small values of K_s.

Now we consider the scheme with implicit approximation of the lowest terms by the Crank–Nicolson method when its first equation takes the form

$$\rho \frac{\hat{v}_z - v_z}{\tau} = \frac{\sigma_{rz}^+ - \sigma_{rz}^-}{h} + \frac{\hat{\sigma}_{rz} + \sigma_{rz}}{2 \, r^0} \ .$$

This scheme is stable over the whole range $0 < K_s \leqslant 1$ and is more accurate when reproducing the near-discontinuity front states compared to the explicit and implicit approximation schemes.

Our comparison of the numerical results for these schemes with those obtained by the controlled energy dissipation scheme leads us to the same qualitative conclusions as in the case of longitudinal cylindrical waves. It was found that the non-conservative difference scheme with approximation of the lowest terms by the Crank–Nicolson method has advantages in the calculation of discontinuities, but is much less accurate than the nondissipative scheme in the case of smooth solutions.

Now we consider the following exact solution of the problem on one-dimensional motion of a cylindrical transverse wave:

$$v_z = \frac{\sigma_0}{\rho \, c_s} \cos \omega t \left(J_2(\xi_s) - \frac{2}{\xi_s} \, J_1(\xi_s) \right), \quad \sigma_{rz} = \sigma_0 \, \sin \omega t \, J_1(\xi_s) \quad \left(\xi_s = \frac{\omega \, r}{c_s} \right).$$

This solution was used to analyze the calculation error. The dimensionless velocity profiles for this solution are shown in Fig. 5 at a fixed time instant for different frequencies.

Tables 5–8 present the errors of the numerical solution. Their analysis show that the use of the Crank–Nicolson approximation scheme (the best one among the explicit schemes being considered) to obtain reliable results requires choosing a finite difference grid in such a way that each half-wave would contain at least 60–70
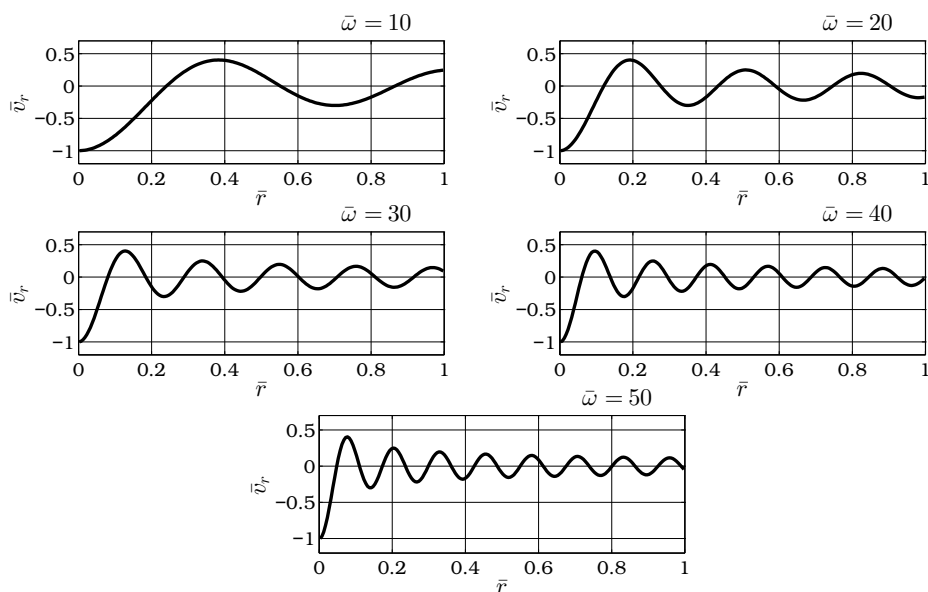
Figure 5. Transverse velocity diagrams for different frequencies

Table 5

Relative errors for the nondissipative scheme: $\gamma = 0$ (transverse waves)

K_s \ $\bar{\omega}$	10	20	30	40	50
0.5	0.00225	0.01931	0.05280	0.101125	0.24425
0.75	0.00097	0.00975	0.02758	0.05381	0.13792
1	0.00097	0.00385	0.00867	0.01589	0.02498
1.25	0.00330	0.02081	0.05215	0.10075	0.24307
1.5	0.00615	0.04155	0.10506	0.20785	0.53001

Table 6

Relative errors for the scheme with explicit approximation of the lowest terms (transverse waves)

K_s \ $\bar{\omega}$	10	20	30	40	50
0.5	0.16838	0.51326	0.64188	0.72456	0.86577
0.75	0.05807	0.24316	0.37495	0.50673	0.74317
1	0.06842	0.19771	0.35433	0.45500	0.46565

Table 7

Relative errors for the scheme with implicit approximation of the lowest terms (transverse waves)

K_s \ $\bar{\omega}$	10	20	30	40	50
0.5	0.19499	0.55547	0.67563	0.73462	0.86316
0.75	0.10331	0.33726	0.47610	0.55343	0.73860
1	0.00956	0.01371	0.01687	0.01968	0.02223

Table 8

Relative errors for the scheme with Crank–Nicolson approximation (transverse waves)

K_s \ $\bar{\omega}$	10	20	30	40	50
0.5	0.18180	0.53469	0.65886	0.72938	0.86436
0.75	0.08090	0.29110	0.42511	0.52797	0.73944
0.97	0.02361	0.04792	0.08386	0.14222	0.21822
1	0.03341	0.09611	0.16719	0.21048	0.21554

grid cells. The nondissipative scheme produces reliable results regardless of the number of half-waves if $K_s \leqslant 1$, but its accuracy decreases as the number of half-waves increases when $K_s > 1$.

Figures 6–8 illustrate the characteristic velocity distributions behind the jump-like front moving in the direction of the symmetry axis and reflecting from the axis. These distributions are obtained according to the scheme with the Crank–Nicolson approximation, by the nondissipative finite difference scheme and by the scheme with a controlled dissipation (for $\gamma = 0.0005$).

5. Torsional waves. One-dimensional torsional waves are described by the following system of equations:

$$\rho\, r\, \frac{\partial v_\varphi}{\partial t} = \frac{\partial(r\, \sigma_{r\varphi})}{\partial r} + \sigma_{r\varphi}\,, \qquad \frac{1}{\mu}\, \frac{\partial \sigma_{r\varphi}}{\partial t} = \frac{\partial v_\varphi}{\partial r} - \frac{v_\varphi}{r}\,. \tag{12}$$

The energy balance equation for this system takes the form

$$\frac{\partial}{\partial t}\left(\rho\, r\, \frac{v_\varphi^2}{2} + r\, \frac{\sigma_{r\varphi}^2}{2\,\mu}\right) = \frac{\partial(r\, v_\varphi\, \sigma_{r\varphi})}{\partial r}\,. \tag{13}$$
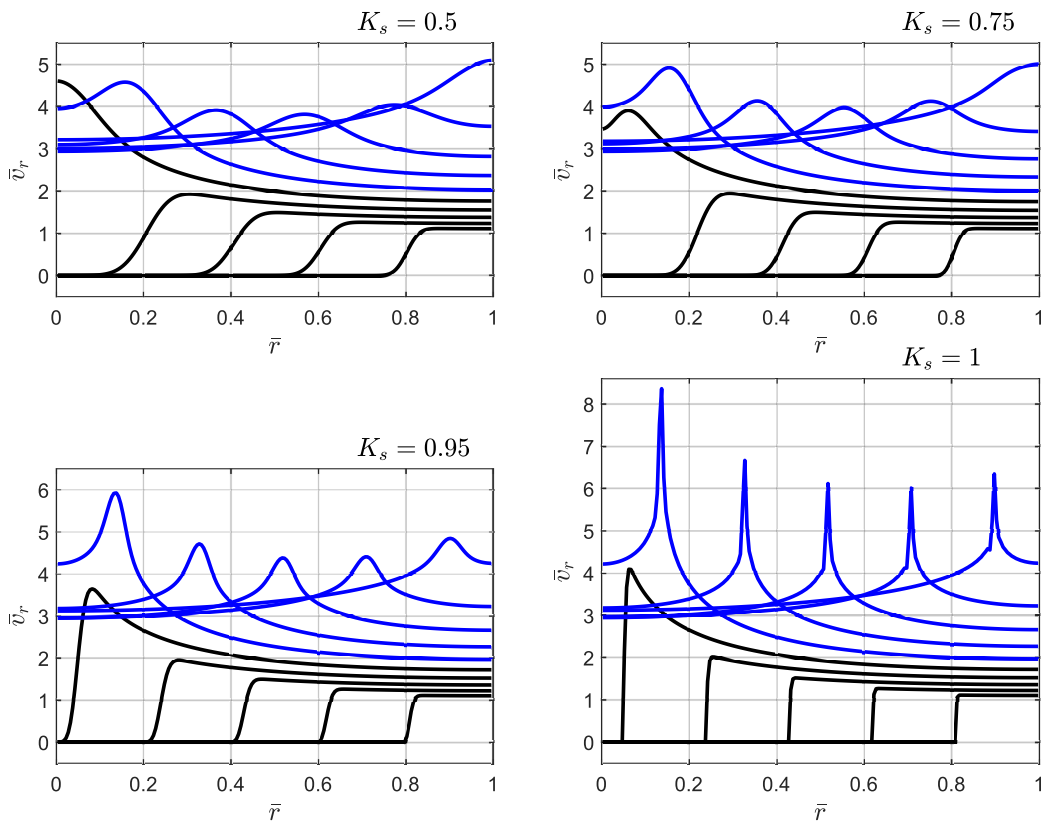
Figure 6. Velocity profiles behind the discontinuity front:
Crank–Nicolson approximation scheme (transverse waves)
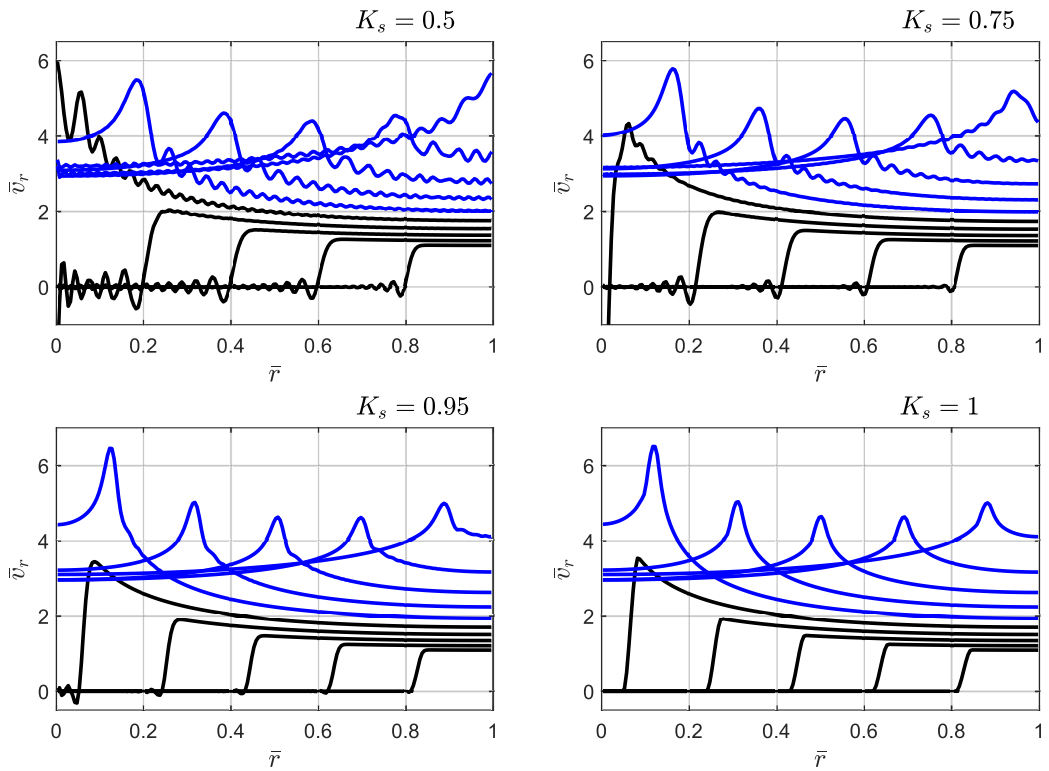
Figure 7. Velocity profiles behind the discontinuity front: nondissipative scheme (transverse waves)
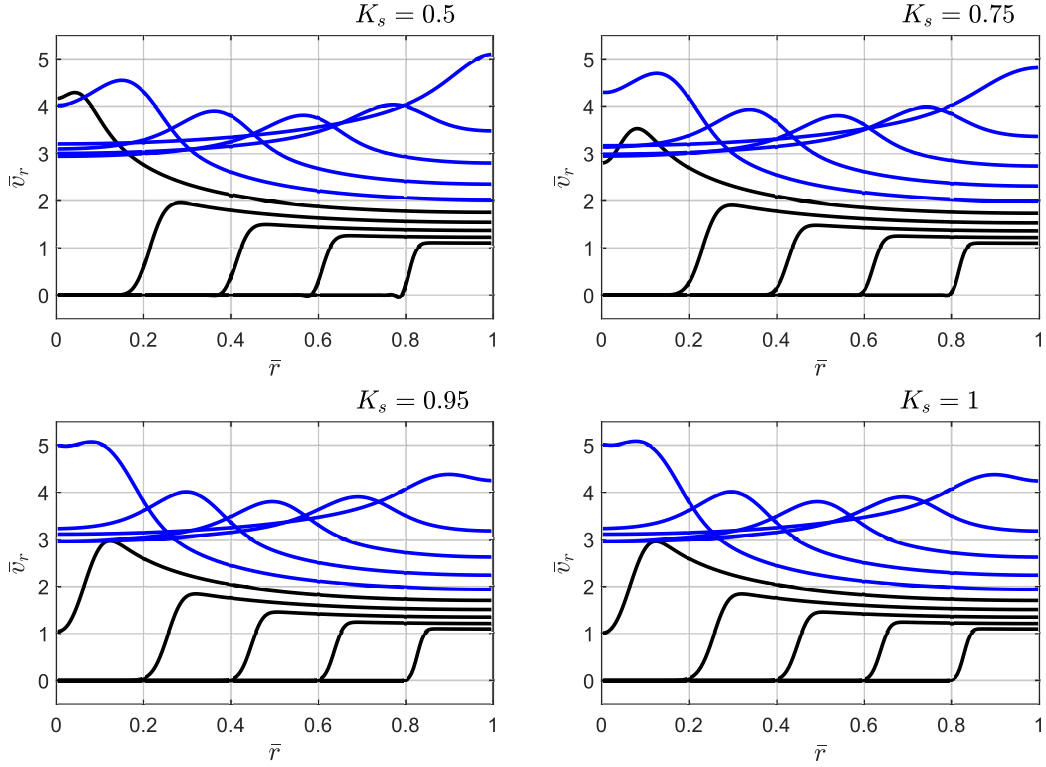
Figure 8. Velocity profiles behind the discontinuity front: a scheme with dissipation (transverse waves)

The discrete analogs of equations (12) and (13) in a cell can be written as

$$\rho\, r^0\, \frac{\hat{v}_\varphi - v_\varphi}{\tau} = \frac{r^+ \sigma_{r\varphi}^+ - r^- \sigma_{r\varphi}^-}{h} + \sigma_{r\varphi}^0\,, \qquad \frac{\hat{\sigma}_{r\varphi} - \sigma_{r\varphi}}{\mu\, \tau} = \frac{v_\varphi^+ - v_\varphi^-}{h} - \frac{v_\varphi^0}{r^0}\,,$$

$$\rho\, r^0\, \frac{\hat{v}_\varphi^2 - v_\varphi^2}{2\tau} + r^0\, \frac{\hat{\sigma}_{r\varphi}^2 - \sigma_{r\varphi}^2}{2\,\mu\,\tau} = \frac{r^+ v_\varphi^+ \sigma_{r\varphi}^+ - r^- v_\varphi^- \sigma_{r\varphi}^-}{h} - D\,,$$

$$D = \frac{r^+ \sigma_{r\varphi}^+ - r^- \sigma_{r\varphi}^-}{h}\left(\frac{v_\varphi^+ + v_\varphi^-}{2} - \frac{\hat{v}_\varphi + v_\varphi}{2} \right)$$

$$+ \frac{v_\varphi^+ - v_\varphi^-}{h}\left(\frac{r^+ \sigma_{r\varphi}^+ + r^- \sigma_{r\varphi}^-}{2} - r^0\, \frac{\hat{\sigma}_{r\varphi} + \sigma_{r\varphi}}{2} \right) - \sigma_{r\varphi}^0\, \frac{\hat{v}_\varphi + v_\varphi}{2} + v_\varphi^0\, \frac{\hat{\sigma}_{r\varphi} + \sigma_{r\varphi}}{2}\,.$$

The closing equations of the "predictor" step are constructed so as to ensure the positive definite quadratic form $D = \gamma\, (v_\varphi^+ - v_\varphi^-)^2 / h^2$ with the dissipation parameter $\gamma \geqslant 0$. They are of the same form as equations (5) if we replace v_r by v_φ and σ_r by $\sigma_{r\varphi}$. After eliminating $\hat{v}_\varphi$ and $\hat{\sigma}_{r\varphi}$, these equations take the form

$$\sigma_{r\varphi}^0 = \frac{\mu\, \tau}{2}\left(\frac{v_\varphi^+ - v_\varphi^-}{h} - \frac{v_\varphi^+ + v_\varphi^-}{2\, r^0} \right) + \sigma_{r\varphi}\,, \qquad \frac{v_\varphi^+ + v_\varphi^-}{2} = \frac{\tau}{2\, \rho\, r^0}\left(\frac{r^+ \sigma_{r\varphi}^+ - r^- \sigma_{r\varphi}^-}{h} + \sigma_{r\varphi}^0 \right) + v_\varphi\,,$$

$$\frac{r^+ \sigma_{r\varphi}^+ + r^- \sigma_{r\varphi}^-}{2} = r^0 \sigma_{r\varphi}^0 + \gamma\, \frac{v_\varphi^+ - v_\varphi^-}{h}\,.$$

They can be reduced to the system

$$r^+ \sigma_{r\varphi}^+ - r^- \sigma_{r\varphi}^- = a_{j-1/2}\, v_\varphi^+ + b_{j-1/2}\, v_\varphi^- + f_{j-1/2}\,, \qquad r^+ \sigma_{r\varphi}^+ + r^- \sigma_{r\varphi}^- = c_{j-1/2}\, v_\varphi^+ + d_{j-1/2}\, v_\varphi^- + g_{j-1/2}$$

with the following coefficients:

$$a_{j-1/2} = \frac{\rho\, h\, r^0}{\tau} - \frac{\mu\, \tau}{2} + \frac{\mu\, \tau\, h}{4\, r^0}\,, \quad b_{j-1/2} = \frac{\rho\, h\, r^0}{\tau} + \frac{\mu\, \tau}{2} + \frac{\mu\, \tau\, h}{4\, r^0}\,, \quad f_{j-1/2} = -2\, \frac{\rho\, h\, r^0}{\tau}\, v_\varphi - h\, \sigma_{r\varphi}\,,$$

$$c_{j-1/2} = \frac{\mu\, \tau\, r^0}{h} - \frac{\mu\, \tau}{2} + \frac{2\, \gamma}{h}\,, \qquad d_{j-1/2} = -\frac{\mu\, \tau\, r^0}{h} - \frac{\mu\, \tau}{2} - \frac{2\, \gamma}{h}\,, \quad g_{j-1/2} = 2\, r^0 \sigma_{r\varphi}\,.$$

In this notation, we again arrive at a tridiagonal system of equations expressed by (7) written with respect to the velocity v_φ. The condition of symmetry $\sigma_{r\varphi} = 0$ for $r = 0$ and the condition for the velocity $v_\varphi = v$ or for the stress $\sigma_{r\varphi} = \sigma$ on the boundary $r = R$ of the domain are added. As in the case of longitudinal or transverse cylindrical waves, these conditions are formulated as equations to be solved together with the main system via the Thomas algorithm.

In this case, the step-by-step computational algorithm repeats the algorithms for the schemes with controlled energy dissipation, as described in the previous sections.

For comparative calculations we considered the grid-characteristic "predictor-corrector" schemes based on the equations

$$\rho\, \frac{\partial v_\varphi}{\partial t} = \frac{\partial \sigma_{r\varphi}}{\partial r} + \frac{2\,\sigma_{r\varphi}}{r}\,, \quad \frac{1}{\mu}\, \frac{\partial \sigma_{r\varphi}}{\partial t} = \frac{\partial v_\varphi}{\partial r} - \frac{v_\varphi}{r}\,.$$

The non-conservative scheme

$$\rho\, \frac{\hat{v}_\varphi - v_\varphi}{\tau} = \frac{\sigma_{r\varphi}^+ - \sigma_{r\varphi}^-}{h} + \frac{2\,\sigma_{r\varphi}}{r^0}\,, \quad \frac{\hat{\sigma}_{r\varphi} - \sigma_{r\varphi}}{\mu\,\tau} = \frac{v_\varphi^+ - v_\varphi^-}{h} - \frac{v_\varphi}{r^0}\,,$$

$$v_\varphi^+ - \frac{\sigma_{r\varphi}^+}{\rho\,c_s} = v_\varphi - \frac{\sigma_{r\varphi}}{\rho\,c_s}\,, \qquad\qquad v_\varphi^- + \frac{\sigma_{r\varphi}^-}{\rho\,c_s} = v_\varphi + \frac{\sigma_{r\varphi}}{\rho\,c_s}$$

with explicit approximation of the lowest terms produces strong oscillations of the solution. These oscillations increase with time (the scheme is unstable) for $K_s = 0.5$ and higher; therefore, it is not reasonable to use it in practice.

The scheme with implicit approximation of the lowest terms obtained by replacing the shear stress $\sigma_{r\varphi}$ and the velocity v_φ by $\hat{\sigma}_{r\varphi}$ and $\hat{v}_\varphi$ and the scheme with approximation of the lowest terms by the Crank–Nicolson method are stable for all $K_s \leqslant 1$.

The relative calculation errors are found by the norm $L_\infty(0, T; L_2(0, R))$ when comparing with the exact solution

$$v_\varphi = \frac{\sigma_0}{\rho\,c_s} \cos \omega t \left(J_3(\xi_s) - \frac{4}{\xi_s}\, J_2(\xi_s) \right), \quad \sigma_{r\varphi} = \sigma_0\, \sin \omega t\, J_2(\xi_s) \quad \left(\xi_s = \frac{\omega\, r}{c_s} \right)$$

to equations (12) for a monochromatic wave with frequency ω. The velocity diagrams for this solution are shown in Fig. 9. Tables 9–11 show the calculation errors for the schemes being considered.

Table 9

Relative errors for the nondissipative scheme: $\gamma = 0$ (torsional waves)

K_s \ $\bar{\omega}$	10	20	30	40	50
0.5	0.00115	0.01481	0.06891	0.18515	0.33317
0.75	0.00045	0.00743	0.03702	0.10161	0.18224
1	0.00070	0.00336	0.00819	0.01496	0.02288
1.25	0.00201	0.01667	0.06618	0.16396	0.27024
1.5	0.00364	0.03322	0.13758	0.34264	0.54504

Table 10

Relative errors for the scheme with implicit approximation of the lowest terms (torsional waves)

K_s \ $\bar{\omega}$	10	20	30	40	50
0.5	0.12927	0.45187	0.81556	0.98173	0.95374
0.75	0.10712	0.33935	0.66174	0.89290	0.90189
1	0.08698	0.18696	0.28001	0.37036	0.43553

The characteristic velocity profiles obtained in our calculations according to the scheme with Crank–Nicolson approximation are illustrated in Fig. 10 and according to the nondissipative scheme are illustrated in Fig. 11. Numerical experiments show that the smoothing of the solution by introducing an artificial dissipation is not required in the case of torsional waves.

Table 11

Relative errors for the scheme with Crank–Nicolson approximation (torsional waves)

$\bar{\omega}$ K_s	10	20	30	40	50
0.5	0.10058	0.42198	0.80260	0.97716	0.95002
0.75	0.05841	0.27131	0.60356	0.84952	0.86860
1	0.02108	0.05058	0.07070	0.09783	0.13319
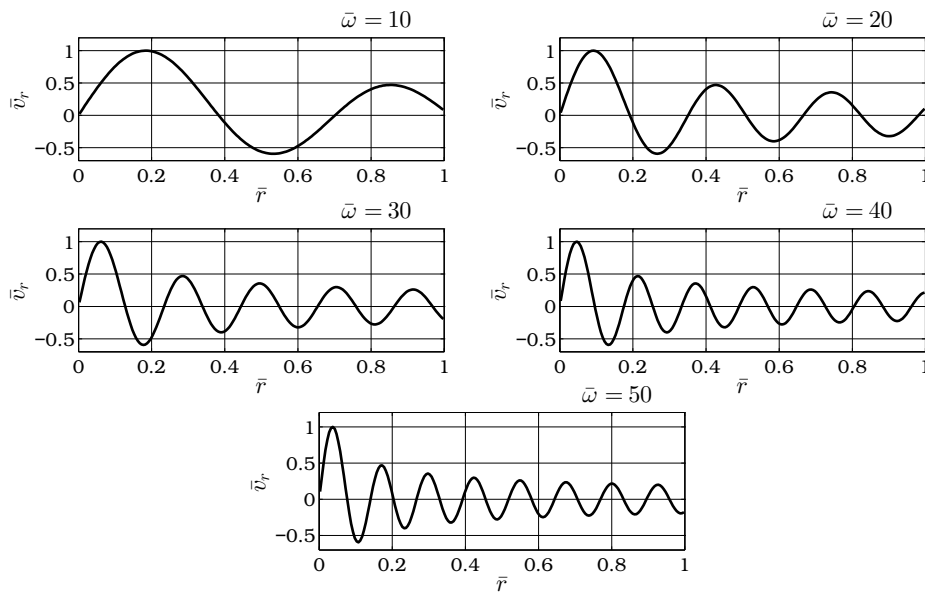
Figure 9. Torsional velocity diagrams for different frequencies

6. Conclusion. Our comparison of the numerical results obtained by the finite difference scheme with controlled energy dissipation with similar results obtained by the typical grid-characteristic "predictor–corrector" schemes shows that the controlled dissipation scheme has a number of advantages in accuracy over other schemes in the case of smooth solutions. The grid-characteristic schemes are preferable for calculating discontinuous solutions due to their monotonicity. The parasitic oscillations during the calculation of discontinuities by the controlled energy dissipation scheme can be smoothed by choosing an adequate artificial dissipation parameter.
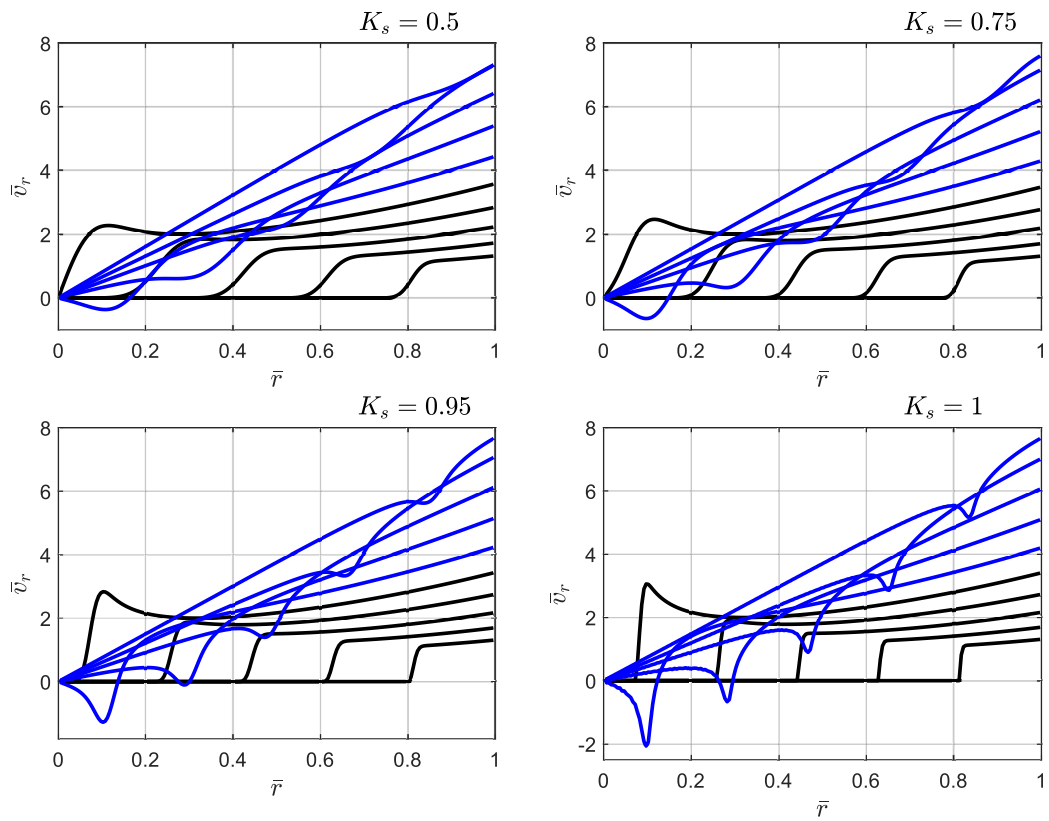
Figure 10. Velocity profiles behind the discontinuity front:
Crank–Nicolson approximation scheme (torsional waves)
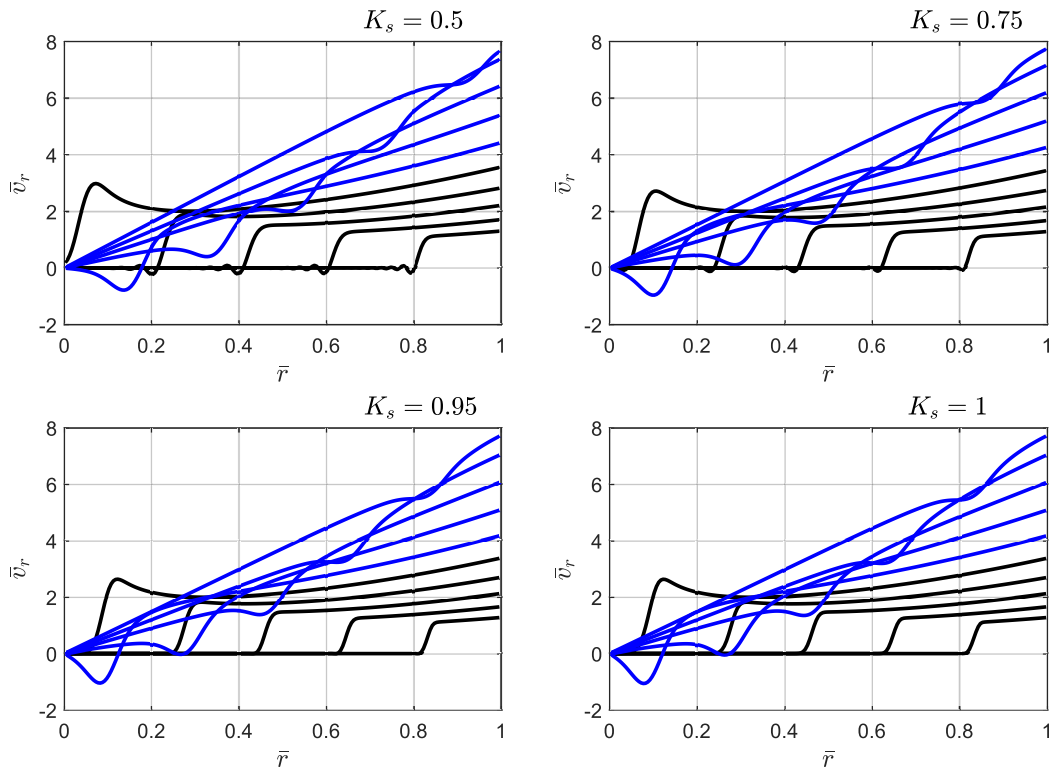
Figure 11. Velocity profiles behind the discontinuity front: nondissipative scheme (torsional waves)

References

1. V. M. Sadovskii, O. V. Sadovskaya, and E. A. Efimov, "Analysis of Seismic Waves Excited in Near-Surface Soils by Means of the Electromagnetic Pulse Source 'Yenisei'," Mater. Phys. Mech. **42** (5), 544–557 (2019).

2. O. V. Sadovskaya and V. M. Sadovskii, "Supercomputing Analysis of Seismic Efficiency of the Electromagnetic Pulse Source 'Yenisei'," in *AIP Conf. Proc.* (American Institute of Physics, College Park, 2019), Vol. 2164, Iss. 1, 110011-1–110011-9.

3. E. A. Efimov, V. M. Sadovskii, and O. V. Sadovskaya, "Mathematical Modeling of the Impact of a Pulse Seismic Source on Geological Media," in *AIP Conf. Proc.* (American Institute of Physics, College Park, 2020), Vol. 2302, Iss. 1, 120002-1–120002-8.

4. S. K. Godunov, A. V. Zabrodin, M. Ya. Ivanov, et al., *Numerical Solution of Multidimensional Problems of Gas Dynamics* (Nauka, Moscow, 1976) [in Russian].

5. S. K. Godunov and V. S. Ryabenkii, *Difference Schemes* (Nauka, Moscow, 1976; North-Holland, Amsterdam, 1987).

6. O. V. Sadovskaya and V. M. Sadovskii, "Parallel Implementation of an Algorithm for the Computation of Elasto-Plastic Waves in a Granular Medium," Vychisl. Metody Programm. **6**, 209–216 (2005).

7. O. Sadovskaya and V. Sadovskii, *Mathematical Modeling in Mechanics of Granular Materials* (Fizmatlit, Moscow, 2008; Springer, Heidelberg, 2012).

8. O. V. Sadovskaya and V. M. Sadovskii, "Numerical Implementation of Mathematical Model of the Dynamics of a Porous Medium on Supercomputers of Cluster Architecture," in *AIP Conf. Proc.* (American Institute of Physics, College Park, 2015), Vol. 1684, Iss. 1, 070005-1–070005-9.

9. V. M. Sadovskii and O. V. Sadovskaya, "Analyzing the Deformation of a Porous Medium with Account for the Collapse of Pores," Zh. Prikl. Mekh. Tekh. Fiz. **57** (5), 53–65 (2016) [J. Appl. Mech. Tech. Phys. **57** (5), 808–818 (2016)].

10. M. P. Varygina, M. A. Pokhabova, O. V. Sadovskaya, and V. M. Sadovskii, "Numerical Algorithms for the Analysis of Elastic Waves in Block Media with Thin Interlayers," Vychisl. Metody Programm. **12** (4), 435–442 (2011).

11. V. M. Sadovskii and O. V. Sadovskaya, "Modeling of Elastic Waves in a Blocky Medium Based on Equations of the Cosserat Continuum," Wave Motion **52**, 138–150 (2015).

12. V. M. Sadovskii, O. V. Sadovskaya, and A. A. Lukyanov, "Modeling of Wave Processes in Blocky Media with Porous and Fluid-Saturated Interlayers," J. Comput. Phys. **345**, 834–855 (2017).

13. V. M. Sadovskii and O. V. Sadovskaya, "Supercomputer Modeling of Wave Propagation in Blocky Media Accounting Fractures of Interlayers," in *Nonlinear Wave Dynamics of Materials and Structures* (Springer, Cham, 2020), Vol. 122, pp. 379–398.

14. P. F. Sabodash and R. A. Cherednichenko, "Application of the Method of Spatial Characteristics to the Solution of Axially Symmetric Problems Relating to the Propagation of Elastic Waves," Zh. Prikl. Mekh. Tekh. Fiz. **12** (4), 101–109 (1971) [J. Appl. Mech. Tech. Phys. **12** (4), 571–577 (1971)].

15. K. M. Magomedov and A. S. Kholodov, *Grid-Characteristic Numerical Methods* (Nauka, Moscow, 1988) [in Russian].

16. I. B. Petrov and A. S. Kholodov, "Numerical Study of Some Dynamic Problems of the Mechanics of a Deformable Rigid Body by the Mesh-Characteristic Method," Zh. Vychisl. Mat. Mat. Fiz. **24** (5), 722–739 (1984) [USSR Comput. Math. Math. Phys. **24** (3), 61–73 (1984)].

17. I. B. Petrov, A. G. Tormasov, and A. S. Kholodov, "On the Use of Hybrid Grid-Characteristic Schemes for the Numerical Solution of Three-Dimensional Problems in the Dynamics of a Deformable Solid," Zh. Vychisl. Mat. Mat. Fiz. **30** (8), 1237–1244 (1990) [USSR Comput. Math. Math. Phys. **30** (4), 191–196 (1990)].

18. V. N. Kukudzhanov, "On Numerical Solution of the Problems of Propagation of Elasto-Viscoplastic Waves," in *Propagation of Elastic and Elastoplastic Waves* (Nauka, Alma-Ata, 1973), pp. 223–230.

19. V. N. Kukudzhanov, *Difference Methods for the Solution of Problems of Mechanics of Deformable Media* (MFTI, Moscow, 1992) [in Russian].

20. V. N. Kukudzhanov, *Numerical Continuum Mechanics* (Fizmatlit, Moscow, 2008; De Gruyter, Berlin, 2013).

21. N. G. Burago, I. S. Nikitin, and A. B. Zhuravlev, "Continuum Model and Method of Calculating for Dynamics of Inelastic Layered Medium," Mat. Model. **30** (11), 59–74 (2018) [Math. Models Comput. Simul. **11** (13), 488–498 (2019)].

22. I. S. Nikitin, N. G. Burago, and A. D. Nikitin, "Explicit–Implicit Schemes for Solving the Problems of the Dynamics of Isotropic and Anisotropic Elastoviscoplastic Media," J. Phys.: Conf. Ser. **1158**, 032039-1–032039-8 (2019).

23. I. S. Nikitin, *Theory of Inelastic Layered and Blocky Media* (Fizmatlit, Moscow, 2019) [in Russian].

24. N. G. Burago and V. N. Kukudzhanov, "A Numerical Method for Solving Axisymmetric Problems for Geometrically Nonlinear Elastic-Plastic Shells of Revolution," Stroit. Mekh. Raschet Sooruzh., N 5, 44–49 (1976).

25. N. G. Burago and V. N. Kukudzhanov, "Buckling and Supercritical Deformations of Elastic-Plastic Shells under Axial Symmetry," in *Collection of Numerical Methods in the Mechanics of Deformable Solids* (Computing Center of the USSR Academy of Sciences, Moscow, 1978), pp. 47–66.

26. V. G. Bazhenov and E. V. Igonicheva, *Nonlinear Processes of Shock Buckling of Elastic Structural Elements in the Form of Orthotropic Shells of Rotation* (Publishing House of UNN, N. Novgorod, 1991) [in Russian].

27. V. G. Bazhenov and D. T. Chekmarev, *Solving Problems of Unsteady Dynamics of Plates and Shells by the Variational-Difference Method* (Publishing House of UNN, N. Novgorod, 2000) [in Russian].

28. V. G. Bazhenov and V. L. Kotov, *Mathematical Modeling of Non-Stationary Processes of Impact and Penetration of Axisymmetric Bodies and Identification of Soil Media Properties* (Fizmatlit, Moscow, 2011) [in Russian].

29. G. I. Marchuk, "Splitting and Alternating Direction Methods," in *Handbook of Numerical Analysis* (Elsevier, North-Holland, 1990), Vol. 1, pp. 197–462.

30. A. G. Kulikovskii, N. V. Pogorelov, and A. Yu. Semenov, *Mathematical Aspects of Numerical Solution of Hyperbolic Systems* (Fizmatlit, Moscow, 2001; CRC Press, Boca Raton, 2001).

31. Yu. P. Popov and A. A. Samarskii, "Completely Conservative Difference Schemes," Zh. Vychisl. Mat. Mat. Fiz. **9** (4), 953–958 (1969) [USSR Comput. Math. Math. Phys. **9** (4), 296–305 (1969)].

32. A. A. Samarskii, *The Theory of Difference Schemes* (Nauka, Moscow, 1977; CRC Press, New York, 2001).

33. B. L. Rozhdestvenskii and N. N. Janenko, *Systems of Quasilinear Equations and Their Applications to Gas Dynamics* (Nauka, Moscow, 1978; American Mathematical Society, Providence, 1983).

34. G. V. Ivanov and V. D. Kurguzov, "Schemes for Solving One-Dimensional Problems of the Dynamics of Inhomogeneous Elastic Bodies on the Basis of Approximation by Linear Polynomials," in *Dynamics of Continuum Medium* (Lavrentyev Inst. of Hydrodynamics, Novosibirsk, 1981), Issue 49, pp. 27–44.

35. G. V. Ivanov, Yu. M. Volchkov, I. O. Bogulskii, et al., *Numerical Solution of Dynamic Elastic-Plastic Problems of Deformable Solids* (Sib. Univ. Izd., Novosibirsk, 2002) [in Russian].

36. V. M. Sadovskii, O. V. Sadovskaya, and E. A. Efimov, "Finite Difference Schemes for Modelling the Propagation of Axisymmetric Elastic Longitudinal Waves," J. Sib. Feder. Univ.: Math. Phys. **13** (5), 644–654 (2020).